Basal Slice Detection Using Long-Axis Segmentation for Cardiac Analysis

Mahsa Paknezhad[1(✉)], Michael S. Brown[2], and Stephanie Marchesseau[3]

[1] National University of Singapore (NUS), Singapore, Singapore
`mahsa@u.nus.edu`
[2] York University, York, Canada
[3] Clinical Imaging Research Centre, A*STAR-NUS, Singapore, Singapore

Abstract. Estimating blood volume of the left ventricle (LV) in the end-diastolic and end-systolic phases is important in diagnosing cardiovascular diseases. Proper estimation of the volume requires knowledge of which MRI slice contains the topmost basal region of the LV. Automatic basal slice detection has proved challenging; as a result, basal slice detection remains a manual task which is prone to inter-observer variability. This paper presents a novel method that is able to track the basal slice over the whole cardiac cycle. The method was tested on 56 healthy and pathological cases and was able to identify the basal slices similar to experts' selection for 80 % and 85 % of the cases for end-diastole and end-systole, respectively. This provides a significant improvement over the leading state-of-the-art approach that obtained 59 % and 44 % agreement with experts on the same input.

Keywords: Basal slice · Long-axis motion · Two-chamber view · Long-axis view · Cardiac analysis · MRI

1 Introduction and Related Work

Analysis of the cardiac function is routinely performed using magnetic resonance imaging (MRI). In a standard cardiovascular MRI scan, three different views of the heart are acquired: a single two-chamber view, a four-chamber view, and a stack of 12–15 short-axis slices covering the whole left ventricle (LV). Important cardiac pathology determinants are stroke volume (SV), ejection fraction (EF), and LV mass which are measured by finding the volume of the LV in the end-systolic and the end-diastolic phases of the cardiac cycle. In order to compute the LV volume, significant progress has been made in developing short-axis segmentation algorithms (e.g. [1]). While these methods give good segmentation accuracy, given the cardiac motion, they often ignore the basal slices which do not have full myocardium around the blood pool. In order to provide an accurate estimate of the LV volume, the most basal slice in the LV must be specified. This can be an issue since manual basal slice specification has been found prone to inter- and intra-observer variability which significantly impacts measured clinical parameters [2,3].

Efforts have been made for automatic basal slice detection. In a recent study, Tufvesson et al. [4] proposed a method to automatically segment the basal short-axis slices considering the long-axis motion of the heart. The approach works by segmenting the basal short-axis slices by considering 24 circumferential sectors over the LV which are analysed individually and removed in case no myocardium is detected. This method is motivated by recently published guidelines by the society for cardiovascular magnetic resonance [5] which indicate that the basal slice is the topmost short-axis slice that has more than 50 % myocardium around the blood cavity. In this approach, the long-axis motion of the heart is also estimated by deforming an LV model based on the segmentations helping to find a more accurate estimation of the volume in the end-systole and end-diastole according to the same guidelines. The algorithm is implemented in the freely available cardiac image analysis software Segment [6] and represents the current state-of-the-art for basal slice detection.

Other methods often exploit the availability of the long-axis views. Notable examples include Lu and Jolly [7] and Mahapatra [8], who proposed methods that train a model by intensity, texture, and contextual features extracted from a bounding box around manually annotated landmarks around the mitral valve in the long-axis view. These methods, however, need further improvement to provide a reliable estimation. There are also trained models of the heart in the literature for segmentation of the left ventricle from different views including the two-chamber view such as the works by Zhuang et al. [9] and Paknezhad et al. [10]. However, these models usually need considerable amounts of training data.

This paper presents a model-free method that relies on the long-axis view to find the basal slice. The long-axis view was chosen as it provides useful information about the base of the LV given the poor quality of the short-axis slices around the base due to heavy blood flow in this area. The proposed approach works by segmenting the LV walls in each slice of the long-axis view and using this segmentation to estimate the basal slice. Consequently, the method is able to provide basal slice identification and long-axis motion estimation over the entire cardiac cycle.

2   Segmenting the Base of the Left Ventricle

The proposed method works by segmenting the basal myocardium walls for the whole time-sequence in the two-chamber view. This is achieved via a two-pass segmentation approach. The first pass is a multi-phase level set that provides an initial segmentation. From the level-set segmentation, seed points are extracted that are used in a random-walk segmentation. The results from these two segmentations are fused to obtain the final basal myocardium wall segmentation. This information is then used to determine the basal slice as described in Sect. 3. The two-pass segmentation approach is described in the following.

User-Input and Pre-processing. The long-axis two-chamber view is selected for segmentation as it provides the clearest view of the LV walls around the
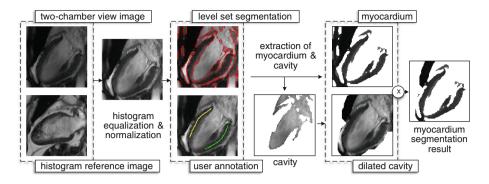
Fig. 1. Steps taken before and after applying the multiphase level set segmentation algorithm on the user-annotated two-chamber view image of the LV.

base. The user is asked to locate the LV walls on an arbitrary two-chamber CINE image by drawing two lines on the LV walls. A 101×101 box is considered around the LV and the histogram of each CINE image is adjusted to a reference image sequence to normalize the contrast.

Multi-phase Level Set. We obtain an initial segmentation using the multi-phase level set algorithm proposed by Li et al. [11]. This segmentation method is deployed since it is capable of following highly varying structures while capturing detailed edges within the image. The algorithm takes intensity inhomogeneity, typical of MRI scans, into account by modeling the relationship between a real-world image I and the true image J as $I = bJ + n$ in which b is a slow-varying bias field that accounts for the intensity inhomogeneities, and n is an additive noise. The final segmentation partitions the true image into N disjoint regions $\Omega_1, \Omega_2, \cdots, \Omega_N$. To estimate the bias field, a circular neighborhood around each pixel y (specified as O_y) is considered. Due to the slow-varying property assumed for the bias field b, the value $b(x)$ for each pixel $x \in O_y$ is approximated to $b(y)$. Since segmentation of the whole image domain Ω into multiple regions $\{\Omega_i\}_{i=1}^N$ partitions the neighborhood O_y, the intensities in the neighborhood of O_y were classified into N clusters with centers $b(y)c_i$ by minimizing the following clustering criterion:

$$\varepsilon_y = \sum_{i=1}^N \int_{\Omega_i \cap O_y} K(y-x)|I(x) - b(y)c_i|^2 \ dx, \tag{1}$$

The N disjoint regions take N constant values $c_1, c_2, \cdots, c_N$ that minimize the energy function. $K(y-x)$ was chosen to be a truncated gaussian function with scale parameter of σ and $K(y-x) = 0$ for $x \notin O_y$. Consequently, The best segmentation was one such that the clustering criterion ε_y was minimized for all $y \in \Omega$. The energy function for the level set was defined as the sum of the clustering criterion ε_y and two regularization terms with μ as the coefficient for the distance regularization term. The algorithm is applied on the user annotated
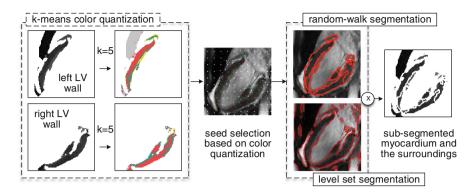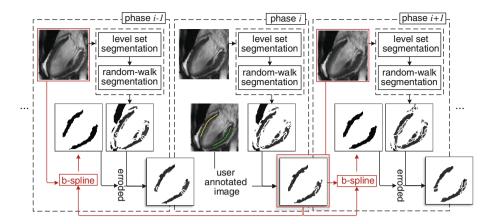
Fig. 2. Selection of seeds for initialization of the random-walk segmentation algorithm by applying k-means color quantization on each wall from the level set segmentation result. The final result is the combination of both segmentation results.

image and the final segments are labeled as left or right wall depending on the user annotation. From this information, the blood cavity of the LV can be estimated and segments that have an average intensity close to the average intensity of the blood cavity are removed. Figure 1 overviews the user annotation and level set segmentation.

Random Walk Segmentation. While the level set segmentation provides a good starting point, we found that it is necessary to further refine the segmentation by integrating the results with the random-walk segmentation algorithm proposed by Grady [12]. The random-walk segmentation algorithm is able to improve the segmentation by subdividing the level set segmentation result into areas with similar intensities and weak edges. This is mainly because the random-walk segmentation is robust to noise and low contrast or absent of boundaries, which make up many of the regions for which level set fails. The drawback of random walk is that it requires user-defined seeds which assign unlabeled pixels to one of the m regions in the image. To this end, we leverage the initial level set results. In particular, the extracted segments from the level set segmentation are smooth and k seed colors are estimated using the color quantization proposed by Verevka [13] as shown in Fig. 2. Areas with similar intensity values are sampled uniformly and assigned the same labels. Samples from the cluster with cluster center close to zero, if any, are assigned similar label as the label for the areas out of the region of interest.

Random walk segmentation works by assigning a label to an unlabeled pixel as the one most likely reached first if a random walker starts from a labeled pixel. This can be treated as a graph problem where the random walker path is biased by assigning weights to the edges which connect the nodes in the graph using the gaussian weighting function $w_{ij} = exp(-\beta(g_i - g_j)^2)$, where w_{ij} is the weight defined for the edge e_{ij} which connects the nodes v_i and v_j and g_i is the image intensity at pixel i. The intensity-related weights prevents the random walker from crossing sharp intensity gradients while moving from one node to

Fig. 3. The segmentation result for the user-annotated (ith) phase is registered to the $(i+1)th$ phase ($(i-1)th$ phase) and used as a mask to select segments from the segmentation result for that phase. The registered mask in the $(i+1)th$ phase ($(i-1)th$ phase) is then registered to the $(i+2)nd$ phase ($(i-2)nd$ phase) and so on.

the other. This algorithm is applied to the two-chamber view image using the assigned labels and the segments which touched the user's annotations were selected and regarded as the final segmentation for the user-annotated image.

Segmentation Propagation. Once the two-pass segmentation is obtained for the user-annotated image, the result is propagated to the other slices in the two-chamber view for segment selection. This is done by using b-spline registration [14] of the initial image to the other images. Segmentation for the other frames is carried out using the same two-pass segmentation approach, however, the warped initial segmentation by the b-spline is used instead of user annotation. This procedure is shown in Fig. 3. The segmentation for each frame is later corrected by incorporating the segmentation results from the two frames before and after the current frame. This temporal consideration helps ameliorate the effects of the noisy segmentation. The top row in Fig. 4 shows the final LV segmentation after this procedure.

3   Estimating the Basal Slice and the Long-Axis Motion

Having segmented the two-chamber view image sequence, the SCMR guidelines [5] are used for basal slice selection. Considering the facts that the line connecting the mitral valve points may not be parallel to the short-axis slices and that multiple short-axis slices may intersect this line, the slice featured by the SCMR guidelines can be approximated to be the topmost short-axis slice below the middle of the line connecting the mitral valve points in the long-axis view. This is mainly because the two-chamber view provides an overview of two opposite walls of LV which are close to the center of the blood cavity. The long-axis motion is also estimated by tracking the relative movement of the mitral
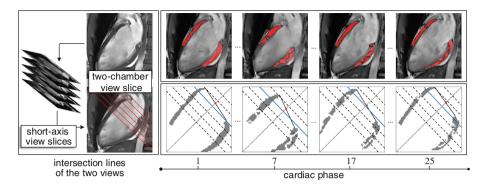
Fig. 4. (Left) Intersections lines between the two-chamber view slice and the short-axis view slices. (Top right) Final segmentation results after correction for a few phases in the cardiac cycle. (Bottom right) Basal slice for each phase. (Color figure online)

valve points along the LV. The bottom row in Fig. 4 shows the position of the basal short-axis slices (dashed lines), the line connecting the mitral valve points (black solid line), and the basal slice (blue line) for several phases for a sample LV. Once the end-diastolic and end-systolic phases are known, the basal slice for those phases can be retrieved and the long-axis motion can be estimated.

4   Evaluation and Results

The method was applied to clinical data from 56 cases, including 30 MRI scans of patients with degenerative mitral valve regurgitation acquired on a Siemens 3T Biograph mMR scanner, 19 MRI scans of healthy subjects acquired on a Siemens 3T Magnetom Trio, and 7 MRI scans of patients with myocardial infarction acquired on a Siemens 3T Magnetom Prisma scanner. The two-chamber cine CMR sequences comprised of 25 phases and the images were 256×232, 192×192, 256×216 pixels in size respectively with resolutions in the range of 1.32–1.56 mm. All 25 images of the two-chamber view were segmented using the proposed method. The number of iterations for the level set segmentation algorithm was set to 10, with scale parameter (σ) of 4, and distance regularization coefficient (μ) of 1. For k-means color quantization, k was set to 5 for all test cases. The weighting parameter (β) for the random-walk segmentation algorithm was set to 30. For images with 1.56 mm resolution, 1.5 times more seeds were sampled for random-walk segmentation. Three hierarchical levels were defined for the b-spline registration algorithm and the mesh window size was set to 10.

For each test case, the basal slice for the end-systole and the end-diastole were retrieved and the long-axis motion was estimated. The results were compared to the manual selections done by consensus between two experts prior to this work. The automatic basal slice selections and long-axis motion estimations by the Segment software [6], as the state-of-the-art approach, were also compared to

the manual selections. In order to compare accuracy of the long-axis motion estimation, the short-axis slices for each test case were segmented using the Segment software [6] and EF, SV, and LV mass were extracted for each case. While using the same short-axis slice segmentations, experts' estimated long-axis motion was input to the Segment manually, so was the long-axis motion measured by the proposed algorithm and the ED, SV, and LV mass were extracted.

Table 1. Comparison of the measured EF, SV and LV mass (LVM) by the Segment tool, our experts and the proposed algorithm. Mean difference error and Pearson's R2 correlation between the two methods and the experts results are also shown. Stars (*) indicate significant differences (p-value<0.001).

		Segment	Experts	Proposed Alg.
EF	mean ± std (%)	62.5 ± 6.8	65.5 ± 6.0	65.2 ± 6.8
	mean diff. error ± std	-2.96 ± 4.55		**-0.22 ± 2.66** *
	R^2 corr.	0.515		**0.702**
SV	mean ± std(ml)	89.7 ± 25.1	96.4 ± 25.3	95.6 ± 27.8
	mean diff. error ± std	-6.63 ± 7.83		**-0.75 ± 6.25** *
	R^2 corr.	0.855		**0.929**
LVM	mean ± std(g)	85.4 ± 25.0	84.1 ± 24.6	84.3 ± 24.6
	mean diff. error ± std	1.34 ± 1.27		**0.15 ± 1.10** *
	R^2 corr.	0.904		**0.975**

From the 56 tested MRI scans, 80 % and 85 % of basal slice selections were found to be identical to the experts' selections for end-diastole and end-systole, respectively. This is while the Segment tool [6] selected the same basal slices as the experts' selected slices for 59 % of the cases in end-diastole and 44 % of the cases in end-systole. The EF, SV, and the LV mass for the proposed algorithm and the Segment tool were compared with those of experts' results using Pearson's R^2 correlation parameter. Table 1 shows the mean and standard deviation for the analysis done by the proposed approach, the Segment tool, and our experts. As can be seen, the mean values for the measured EF, SV, and LV mass by the proposed algorithm are closer to those of experts' measurements. It also shows the Pearson's R^2 correlation values for both methods. For all three parameters, the proposed algorithm provided more similar results to experts' analysis results. The average execution time for the proposed algorithm was 30 s for a non-optimized Matlab code with user input time of 9 s.

5   Discussion and Conclusion

Due to the high anatomical variability of the heart as well as the resolution and contrast limitations of MR scans, landmark-based approaches have not been able to accurately distinguish and locate mitral valve points using feature extraction methods. Model-based segmentation approaches also require considerable

amount of training data. Consequently, an image-driven segmentation approach for basal LV segmentation was proposed in this paper providing accurate segmentation of the area around the mitral valve points. The proposed method does not require model training. The proposed approach is able to detect the basal slice through the whole cardiac cycle as well as estimate the long-axis motion of the heart which are essential to provide a robust and accurate method for cardiac analysis. Although our method is semi-automatic, the required user input has minimum influence on the final results since it only guides selection of the cluster of segments to include for volume measurement. Future work will remove the currently required user input.

References

1. Ben Ayed, I., Punithakumar, K., Li, S., Islam, A., Chong, J.: Left ventricle segmentation via graph cut distribution matching. In: Yang, G.-Z., Hawkes, D., Rueckert, D., Noble, A., Taylor, C. (eds.) MICCAI 2009, Part II. LNCS, vol. 5762, pp. 901–909. Springer, Heidelberg (2009)
2. Marcus, J.T., Gtte, M.J.W., DeWaal, L.K., Stam, M.R., Van der Geest, R.J., Heethaar, R.M., Van Rossum, A.C.: The influence of through-plane motion on left ventricular volumes measured by magnetic resonance imaging: implications for image acquisition and analysis. J. Cardiovasc. Magn. Reson. **1**(1), 1–6 (1999)
3. Marchesseau, S., Ho, J.X.M., Totman, J.J.: Influence of the short-axis cine acquisition protocol on the cardiac function evaluation: a reproducibility study. Eur. J. Radiol. **3**, 60–66 (2016)
4. Tufvesson, J., Hedstrm, E., Steding-Ehrenborg, K., Carlsson, M., Arheden, H., Heiberg, E.: Validation and development of a new automatic algorithm for time-resolved segmentation of the left ventricle in magnetic resonance imaging. BioMed Res. Int. 970357 (2015)
5. Schulz-Menger, J., Bluemke, D.A., Bremerich, J., Flamm, S.D., Fogel, M.A., Friedrich, M.G., Nagel, E.: Standardized image interpretation and post processing in cardiovascular magnetic resonance: society for cardiovascular magnetic resonance (SCMR). J. Cardiovasc. Magn. Reson. **15**(35), 1167–1186 (2013)
6. Heiberg, E., Sjgren, J., Ugander, M., Carlsson, M., Engblom, H., Arheden, H.: Design and validation of segment a freely available software for cardiovascular image analysis. BMC Med. Imaging **10**(1) (2010)
7. Lu, X., Jolly, M.-P.: Discriminative context modeling using auxiliary markers for LV landmark detection from a single MR image. In: Camara, O., Mansi, T., Pop, M., Rhode, K., Sermesant, M., Young, A. (eds.) STACOM 2012. LNCS, vol. 7746, pp. 105–114. Springer, Heidelberg (2013). doi:10.1007/978-3-642-36961-2_13
8. Mahapatra, D.: Landmark detection in cardiac MRI using learned local image statistics. In: Camara, O., Mansi, T., Pop, M., Rhode, K., Sermesant, M., Young, A. (eds.) STACOM 2012. LNCS, vol. 7746, pp. 115–124. Springer, Heidelberg (2013). doi:10.1007/978-3-642-36961-2_14
9. Zhuang, X., Rhode, K.S., Razavi, R.S., Hawkes, D.J., Ourselin, S.: A registration-based propagation framework for automatic whole heart segmentation of cardiac MRI. IEEE TMI **29**(9), 1612–1625 (2010)
10. Paknezhad, M., Marchesseau, S., Brown, M.S.: Automatic basal slice detection for cardiac analysis. In: SPIE 9784, Medical Imaging: Image Processing (2016)

11. Li, C., Huang, R., Ding, Z., Gatenby, J.C., Metaxas, D.N., Gore, J.C.: A level set method for image segmentation in the presence of intensity inhomogeneities with application to MRI. IEEE TIP **20**(7), 2007–2016 (2011)
12. Grady, L.: Random walks for image segmentation. IEEE PAMI **28**(11), 1768–1783 (2006)
13. Verevka, O.: The Local K-means Algorithm for Colour Image Quantization. Pro-Quest Dissertation Publishing (1995)
14. Myronenko, A., Song, X.: Intensity-based image registration by minimizing residual complexity. IEEE PAMI **29**(11), 1882–1891 (2010)